

CONUS Contrail Frequency and Coverage Estimated from RUC and Flight Track Data

David P. Duda, Hampton University

NASA Langley Research Center
Mail Stop 420
Hampton, VA 23681-2199 USA
Email: d.p.duda@larc.nasa.gov

Patrick Minnis, Atmospheric Sciences, NASA LaRC
Donald P. Garber, Atmospheric Sciences, NASA LaRC

NASA Langley Research Center
Mail Stop 420
Hampton, VA 23681-2199 USA
Email: p.minnis@larc.nasa.gov, d.p.garber@larc.nasa.gov

Rabindra Palikonda, Analytical Services and Materials, Inc.

One Enterprise Parkway, Suite 300
Hampton, VA 23666 USA
Email: r.palikonda@larc.nasa.gov

(Article submitted to Meteorologische Zeitschrift February 2004)

Corresponding author: Dr. David P. Duda, NASA Langley Research Center, Mail Stop 420,
Hampton, VA 23681-2199 USA. Email: d.p.duda@larc.nasa.gov.

Abstract. Estimates of contrail frequency and coverage over the continental United States (CONUS) are developed using hourly meteorological analyses from the Rapid Update Cycle (RUC) numerical weather prediction model and commercial air traffic data for 2 months during 2001. The potential contrail frequency over the CONUS is computed directly from RUC analyses using several modified forms of the classical Appleman criteria for persistent contrail formation. Various schemes for diagnosing contrails from the RUC analyses were tested by first tuning each model to mean satellite estimates of contrail coverage for the domain and then comparing the resulting distributions to those from the satellite retrievals. The most accurate method for forming persistent contrails for both months uses a square root relationship between flight lengths and contrail coverage, accounts for contrail overlap and for the dry bias in the humidity profiles, and assumes that contrails can be detected in all conditions. The differences between the simulated and observed contrail amounts are due, to errors in the observations, possible diurnally dependent saturation effects, and uncertainties in the numerical weather analysis humidity fields and other input variables. The algorithms developed here are suitable for eventual application to real-time predictions of potential contrail outbreaks. When refined, the methodology could be useful for both contrail mitigation and for contrail-climate effects assessment.

Zusammenfassung

Schätzungen der Kondensstreifen-Frequenz und Einschusses über die kontinentalen Vereinigten Staaten (CONUS) werden entwickelt, stündlich meteorologische Analysen vom Schnellen Aktualisierungszyklus (RUC) numerisches Wetter-Vorhersage-Modell und kommerzielle Luftverkehr-Daten seit 2 Monaten während 2001 gebrauchend. Die potenzielle Kondensstreifen-

Frequenz über den CONUS wird direkt von RUC-Analysen geschätzt, die mehrere modifizierte Formen der klassischen Appleman Kriterien für die beharrliche Kondensstreifen-Bildung gebrauchen. Verschiedene Schemas, um Kondensstreifen von den RUC-Analysen zu diagnostizieren, wurden durch die erste Einstimmung jedes Modells geprüft, um Satellitenschätzungen des Kondensstreifen-Einschlusses für das Gebiet und das dann Vergleichen vom resultierenden Vertrieb zu denjenigen von den Satellitenwiederauffindungen zu bedeuten. Die genaueste Methode, um beharrliche Kondensstreifen seit beiden Monaten zu bilden, gebraucht eine Quadratwurzelbeziehung zwischen Fluglängen und Kondensstreifen-Einschluss, Rechnungen für Kondensstreifen-Übergreifen und für die trockene Neigung in den Feuchtigkeitsprofilen, und nimmt an, dass Kondensstreifen in allen Bedingungen entdeckt werden können.

1. Introduction

Contrails can affect the global atmospheric radiation budget by increasing planetary albedo and reducing infrared emission. Our current knowledge of the magnitude of these effects is extremely uncertain; two recent estimates of global linear contrail radiative forcing (MINNIS et al. 1999, PONATER et al. 2002) differ by nearly two orders of magnitude. Global radiative forcing is difficult to estimate since it depends on several poorly known factors including the global mean contrail coverage. Current theoretical estimates of global contrail coverage (SAUSEN et al. 1998, PONATER et al. 2002) are tuned to early values of linear contrail coverage determined visually from infrared satellite imagery over the North Atlantic and central Europe (BAKAN et al. 1994). The estimates differ based on the parameterization used to diagnose contrails and the numerical weather analyses employed to determine the ambient conditions. Contrail coverage recently derived over those same areas using an objective detection algorithm (MANNSTEIN et al. 1999, MEYER et al. 2002) are significantly smaller than those given by BAKAN et al. (1994). A comparison of the empirical contrail coverage of SAUSEN et al. (1998) with those from analyses of Advanced Very High Resolution Radiometer (AVHRR) data taken over the continental United States (CONUS) (PALIKONDA et al. 1999) and the northeastern Pacific (MINNIS ET AL. 2004) show that they are similar in overall magnitude, but differ in spatial distribution. Contrail coverage over the CONUS during 2001, however, differs significantly from the theoretical estimates in both magnitude and distribution (PALIKONDA et al. 2004) These results illustrate the current uncertainty in contrail coverage estimation, a key component in the determination of contrail climate effects.

Development of reliable methods for diagnosing persistent contrails and their physical and radiative properties from numerical weather analyses is essential for predicting future

contrail climate impacts. Because air traffic is expected to grow by 2 to 5% annually (MINNIS et al. 1999), it is important to estimate contrail coverage accurately. As another step in addressing this concern, actual flight data and coincident meteorological data are used in this paper to estimate contrail coverage over the CONUS for a 2 months using a variety of diagnosis schemes. The estimates are compared with satellite retrievals of contrail coverage based on an objective contrail detection algorithm to determine the most accurate contrail formation scheme and to identify the deficiencies in the methodology and input that need further improvement.

2. Data

2.1 Air traffic data

A commercial air traffic database compiled by GARBER et al. (2004) was used to specify air traffic density over the CONUS during September and November, 2001. The database consists of 2 or 5-minute readings of aircraft (flight number, aircraft type), position (latitude, longitude, altitude), and heading for every non- military flight over the USA and a portion of Canada, including related transoceanic flights. Although the database does not include military flights, it contains most of the air traffic over the CONUS. Air traffic densities were tabulated in terms of cumulative flight path lengths per $1^{\circ}\times 1^{\circ}$ region at a vertical resolution of 1 km. The domain extends from 20°N to 50°N and from 135°W to 60°W .

2.2 Meteorological and satellite data

Atmospheric profiles of temperature and humidity were derived from the 40-km resolution, 1-hourly Rapid Update Cycle (RUC) analyses (BENJAMIN et al. 2004) in 25-hPa intervals from 400 hPa to 150 hPa. The RUC data were linearly interpolated at each pressure level into a $1^{\circ}\times 1^{\circ}$ grid that extends from 25°N to 56°N and from 129°W to 67°W .

The RUC analyses at 00 UTC and 12 UTC were not used in this study to insure that the humidity fields for each hour were consistent. Before February 2002, a “quick-look” version of the 00 UTC and 12 UTC analyses was collected that did not include all available radiosonde data. It is noticeably drier in the upper troposphere than the analyses from other hours.

A major revision to the operational RUC model was implemented 17 April 2002. The RUC20 model with 20-km horizontal resolution replaced the 40-km resolution RUC40 model. To improve quantitative precipitation forecasts, several changes in the way the model handles upper tropospheric moisture were made. The tropopause is more sharply defined, and most ice supersaturations for pressure levels less than 300 hPa are removed (BENJAMIN et al. 2004). These changes dry the upper troposphere relative to that in the RUC40. Thus, the relative humidity thresholds used to make the contrail diagnoses for the RUC40 data were changed for the RUC20. Nearly simultaneous RUC20 (19 UTC) and RUC40 (20 UTC) model analyses from 26 May 2002 were used to relate the RUC20 humidity data to the older RUC40 data. The relative humidities with respect to ice (RHI) from the RUC20 analyses were adjusted based on a level-by-level comparison of the mean RHI computed from the RUC20 and RUC40 data.

The satellite datasets for deriving contrail and cloud coverage consist of infrared radiances from the Sun-synchronous *NOAA-16* AVHRR 1-km imager (10.8 and 12.0 μm) and multi-spectral 1-km data from the MODerate Resolution Imaging Spectroradiometer (MODIS) on the *Terra* satellite (BARNES et al. 1998). The MODIS data were used to determine areas of cloudiness that may obscure contrail detection.

3. Method

Persistent contrail formation was computed according to the classical criteria of APPLEMAN (1953) using the RUC profiles of temperature and humidity. The contrail formation algorithm follows SCHRADER (1997), modified with the aircraft propulsion efficiency parameter of BUSEN and SCHUMANN (1995). The mean value of the propulsion efficiency assumed for the present commercial fleet was 0.30 (SAUSEN et al. 1998). The saturation vapor pressure coefficients of ALDUCHOV and ESKRIDGE (1996) [AERW(50,-80) and AERWi(0,-80)] were used to compute saturation vapor pressure over water and ice.

According to classical contrail formation theory, contrails can persist when the ambient air is supersaturated with respect to ice (that is, the environmental RHI is greater than 100%), but not with respect to water. In SAUSEN et al. (1998), the use of ECMWF reanalysis data required a contrail parameterization to compute persistent contrail coverage since the RHI values in the ECMWF model rarely exceed 100%. The RUC model contains a sophisticated cloud and moisture scheme that allows for ice-supersaturation. Assuming that the RUC upper tropospheric moisture variables are accurate, we can follow a much simpler statistical evaluation of potential persistent contrail frequency. For each $1^\circ \times 1^\circ$ grid box where the criteria for persistent contrails occur at any level from 400 hPa to 150 hPa, a persistence indicator is given a value of 1 for each hourly analysis. The indicator equals zero when none of the levels satisfies the persistence criteria. The potential contrail frequency (PCF) over a time period becomes simply the frequency of occurrence of the persistence indicator at a particular location. DUDA et al. (2004) demonstrated that the RUC underestimates upper tropospheric humidity by showing that persistent contrails developed in regions where the RUC40 computed an RHI of only 85%. Additional simulations (not shown here) indicate that although adjusting the contrail formation

criteria to a lower RHI increases contrail coverage, the change does not significantly affect the overall pattern of the CONUS contrail coverage.

To compute the actual contrail coverage, the PCF must be multiplied by the air traffic density. For an initial estimate, we will assume initially that the air traffic density is sparse enough to relate the contrail fractional coverage to the total air travel linearly. The unknown quantity is the mean fractional persistent contrail coverage, c_{flt} , that results from each kilometer of air travel within a given area. In this study c_{flt} was initially tuned to match the CONUS mean contrail coverage from monthly satellite-based contrail coverage estimates (PALIKONDA et al. 2004) as well as uniformly adjusting the RHI threshold to 100% for contrail formation regardless of air temperature. Only satellite-derived contrail coverage actually measured within the CONUS borders was used for the tuning. The linear-based value of c_{flt} varied by 20% between September 2001 (3.72×10^{-5}) and November 2001 (4.49×10^{-5}). No overlap of the contrails is assumed in this simple estimate because contrail altitude is not considered. The total persistent contrail coverage (c_{sum}) in a grid cell is simply

$$c_{sum} = PCF \times c_{flt} \times n \tag{1}$$

where PCF is the potential contrail frequency for the column between 400 and 150 hPa, c_{flt} is the mean fractional persistent contrail coverage per distance traveled within a grid cell, and n is the total cumulative path length for flights between 400 and 150 hPa within a grid cell.

To account for the effects of natural cloudiness obscuring the detection of contrails, the persistence indicator used in the computation of PCF was set to zero whenever a grid box was more than 50% covered by high cloud. High cloud coverage (cloud tops > 5 km) for September and November 2001 was derived from *Terra* MODIS multi-spectral observations (MINNIS et al. 2002). Figure 1 shows the distribution of ice-cloud amount, a quantity accounting for most

Fig. 1

clouds above 5 km, observed around 1030 LT from *Terra*. The upper troposphere was relatively dry over the CONUS during September as indicated by the small amounts of cirrus coverage. The broad maximum off the Atlantic coast resulted from the passage of a tropical storm. During November, cirrus maxima occurred over southeastern Canada and northwestern CONUS.

4. Results

4.1 Potential contrail frequency

Figure 2 presents the potential contrail frequency computed for September and November 2001. RUC analyses were available for only 26 of 30 possible days during each month. For both months, maximum PCF occurred over the northwestern CONUS, where values reach 0.33 in September and 0.50 in November. Another region of high frequency during November is the eastern half of the CONUS centered over the confluence of the Mississippi and Ohio Rivers. The prevailing synoptic-scale weather patterns during each month strongly influence the overall distribution and magnitude of the monthly potential contrail frequency. The mean PCF for grid points over the CONUS was 0.118 in September and increased to 0.272 in November. These amounts are comparable to the 11-year average (0.141) over the US computed by SAUSEN et al. (1998).

Fig. 2

Figure 3 shows the PCF computed for both months using the available afternoon (~1430 LT) overpasses of the *NOAA-16* satellite. To approximate the satellite coverage in the calculation of the contrail frequencies, only grid points within $\pm 12^\circ$ of longitude of the sub-satellite point at 37°N were counted during each overpass. Although the mean potential contrail frequencies computed for the CONUS were almost identical to the monthly averages (0.139 for

Fig. 3

September 2001, 0.270 for November 2001), the distribution of PCF is much more variable in Figure 3 than in Figure 2 due to the limited sample sizes.

The PCFs should be related to the occurrence of natural cirrus clouds because the conditions giving rise to cirrus clouds are similar to those for contrail formation except for the lower RHI contrail formation threshold and the low temperature requirement for contrails. During both months the ice cloud (Fig. 1) and PCF (Fig. 2) patterns are generally similar with some notable exceptions. The differences between the September and November ice cloud amounts (Fig. 1) over the northwestern CONUS are not consistent with the calculation of similar PCFs during both months (Fig. 2). This inconsistency suggests that the RUC overestimates RHI over the northwestern CONUS during September. During November, the orientation of the axes of maximum cirrus and PCF over the Ohio River Basin are very similar, but the cirrus axis occurs farther west than its PCF counterpart. The PCF maximum is broader with the 26% contour extending eastward over the southeastern coast while the cirrus coverage decreases over the same areas.

To further check the quality of the RUC-based potential contrail frequencies, they were compared to a daily, manual analysis of CONUS contrail coverage based on 4-km imagery from the eighth Geostationary Operational Environmental Satellite (*GOES-8*). The 10.8 μm minus 12.0 μm brightness temperature difference images between 1045 UTC and 0045 UTC were examined for the occurrence of contrails within each state of the CONUS. For each day of the analysis, a persistence indicator value of 1 was given for each state in which at least one contrail appeared. The contrail frequency for each state is simply the percentage of the total analyzed days with contrail occurrence. The monthly mean contrail frequency for all states in the CONUS region was defined as the observation index. The comparison is shown in Figure 4.

Fig. 4

As expected, the contrail frequencies computed from the RUC model are higher than the observation index since the index is based on observations of 4-km resolution data that likely miss narrow contrails. In addition, any satellite-based estimate is affected by the obscuration of contrails from natural clouds. The potential contrail frequencies and the observation indices have similar seasonal cycles except after April 2002 when the RUC20 model data were used. The apparent correlation between the model contrail frequency and the *GOES-8* index abruptly disappears at that point. The divergence in PCF and the *GOES-8* index during this period is likely the result of changes in the convective parameterization and ice cloud formation model introduced in the RUC20. The RUC40 allowed the development of relatively large, realistic supersaturations while the RUC20 set the RHI = 100% wherever the model diagnosed a cloud and converted the remaining regions to RHI = 80% resulting in less realistic probability distributions of RHI. Because of the correlation between PCF and the *GOES-8* index, only RUC40 data are considered hereafter.

4.2 Contrail coverage

To facilitate comparisons between observations and simulations, Figures 5 and 6 show plots of simulated persistent contrail coverage c_{sum} and satellite-observed contrail coverage for September and November 2001. The value of c_{sum} was computed using two different assumptions: contrail coverage is linearly proportional to air traffic density and it is proportional to the square root of air traffic density. Results from the two approaches, hereafter denoted as linear and square-root, are plotted in the panels (a) and (c) for each figure. The satellite-based CONUS contrail coverage estimates, shown in the (b) panels, used *NOAA-15* & *NOAA-16* AVHRR data and an objective contrail detection algorithm (MANNSTEIN et al. 1999) to compute

Fig. 5

Fig. 6

contrail coverage (PALIKONDA et al. 2004). The simulated coverage is heavily influenced by the air traffic density pattern, and is similar in appearance to SAUSEN et al. (1998), with a maximum in the eastern half of the CONUS, and relatively little coverage in the northern Great Plains. The simulated coverage for September also has a maximum in the northwestern states that reflects the extremely high PCF in the area computed at the satellite overpass times. The contrail coverage for the CONUS based on the objective satellite analysis is 0.37% for September 2001 and 1.02% for November 2001. The linearly simulated contrail coverage (Figs. 5a and 6a) yields larger maxima compared to the square root coverage. No relative maxima are evident over the Pacific, Canada, or Mexico due to limited flight information in those areas. The greatest concentrations of simulated contrails appear over the southeastern states and the central Mississippi basin.

The satellite results from both months (Figs. 5b and 6b) appear to be more dependent on the PCF (in other words, the environmental conditions) than the estimates in Figures 5a and 6a (which are strongly influenced by air traffic patterns). Several unresolved factors may account for this difference. For example, in high air traffic regions, it is likely that contrail coverage is non-linearly related to air traffic density due to “saturation” effects (i.e. competition for moisture or overlapping of contrails in air traffic corridors may limit the number of linear contrails that are visible by satellite). If a square-root relation between coverage and air traffic is assumed, the contrail coverage is less dependent on air traffic density (SAUSEN et al. 1998). Also, the current analyses used for Figures 5a and 6a do not consider the effects of the temperature dependence of the dry bias in upper tropospheric soundings (MILOSHEVICH ET AL. 2001) that are likely to influence the RUC analyses. If the contrail detection algorithm is not significantly affected by underlying cloudiness, the cloud mask used in the simulated-linear analyses may be unnecessary.

Indeed, contrails are often detected in both thin and thick cirrus clouds (e.g., PALIKONDA et al. 2004).

To account for these factors, the flight track and RUC data were binned into four altitude regions (7-9 km, 9-11 km, 11-13 km, and 13-15 km), and contrail coverage was computed for each layer. To calculate the total contrail coverage, the coverage for each layer was summed using the random overlap assumption. In addition, a temperature-dependent RHI threshold was used to compute the PCF. The threshold was set to 100% for temperatures of -40°C or higher, and decreases linearly with temperature at a rate of $1\%/^{\circ}\text{C}$ between -40°C and -70°C . For temperatures below -70°C the threshold was 70%. The cloud mask used in Figures 5a and 6a was turned off, and finally, the coverage in each layer was assumed to be proportional to the square root of the air traffic distance flown in each grid box.

The simulated square-root coverages for September and November 2001 are shown in Figures 5c and 6c. Although the square-root coverage compares better than the linear simulation with the satellite-derived coverage, many significant differences remain. Figures 7a and 7b show the observed minus the square-root simulated coverage for September and November 2001 over the CONUS. The simulated September coverage compares well with the satellite-based coverage over much of the eastern third of the US, although the satellite analysis has a maximum over the northeastern states, which may be the result of cirrus streamer contamination due to tropical storms during the month. The simulated coverage also has a strong maximum over Washington and Oregon that is not seen in the satellite analysis. This maximum results from the extremely large PCF computed for this region at all levels, and may be an artifact of the RUC analysis during this month. As noted earlier, the RUC appears to overestimate upper tropospheric humidity over the northwest during September and over the southeastern CONUS during

November. Figures 5b and 6b have maxima over the northern Plains, New York, Pennsylvania and southern New England that are not in the simulated results.

Figure 7a shows that the satellite-observed coverage is much higher in a region extending from northern California through the northern Rockies into northern Minnesota. Some of this difference may be due to the presence of military traffic in this region of the CONUS that is not available in the flight track database (BJORNSON, 1992). The simulated coverage may also be lower in these regions due to false contrail detection due to cumulus cloud streets and mountain-valley features that are typically mistaken as contrails by the automated algorithm (e.g., MINNIS et al. 2004). A similar difference between the observed and simulated coverage in this region also appears in Figure 7b. Figure 7 shows that the simulated coverage appears to be larger than that observed over the central Plains states for both months. This region is in the lee of the Rocky Mountains where negative vertical velocities induced by the topography may suppress the development of contrails in this region. The root mean square (RMS) difference between the observed and square-root simulated contrail coverage was 0.27% for September and 0.60% for November 2001.

5. Discussion

A new estimate of the linear contrail coverage over the continental United States is computed by combining for the first time hourly temperature and humidity analyses from an operational numerical weather prediction model with actual commercial air travel statistics. Potential contrail frequencies (PCF) are computed directly from the meteorological data using classical contrail formation criteria. PCFs for two months are presented, and show large variations in magnitude depending on the synoptic-scale pattern. The PCFs computed during

NOAA-16 overpasses suggest that potential contrail frequency is not strongly influenced by the time of the satellite observation.

Assuming a simple linear relation between contrail coverage and the total air traffic distance flown, persistent contrail coverage is computed for both months. The simulated persistent contrail coverage presented here is heavily influenced by the air traffic pattern, similar to earlier studies. The small magnitude of the c_{fl} parameter reveals that even in areas suitable for contrail formation, only a small fraction of all flights produce persistent contrails that are detectable by satellite. The contrail coverage computed from *NOAA-16* imagery, however, is more closely related to the potential contrail frequency (and high cloud coverage) than to air traffic density. This suggests that the coverage of linear contrails is non-linearly related to air traffic, and “saturation” effects are important in high traffic areas.

Several factors were tested to determine their effects on the simulation of contrail coverage, and the results of these tests were used to produce the improved square-root simulation discussed above. In addition to the 100% RHI threshold presented here, thresholds of 85% and 70% were also used to compute PCF and the simulated contrail coverage. Lowering the RHI threshold tended to smooth out the simulated coverage, and to increase the contrail coverage in the eastern CONUS relative to that in the west, but the overall pattern of simulated coverage remained dominated by the air traffic density pattern. The assumption that the contrail coverage was proportional to the fourth root of the air traffic density was also considered. This relation produced simulated coverages similar to those using the square root relation, but might be physically unrealistic. The increased vertical resolution of the air traffic and humidity data in the square-root simulations appeared to affect the results in the west more than in the eastern CONUS. The greater improvements in the western regions may result from the relatively

smaller amounts of air traffic over the area. Three cloud masks were used in an attempt to screen out areas supporting contrails that were likely to be undetectable by satellite. One cloud mask eliminated areas where all cloud coverage exceeded 50%, another removed grid points with optically thick clouds ($\tau > 5$) and a third masked regions with optically thick and high (cloud tops > 5 km) clouds.

An overall assessment of the results is summarized in Table 1, which lists the RMS differences between the observed and simulated contrails for most of the diagnosis schemes discussed above. Clearly, the two extremes are shown in Figures 5 and 6. The linear relationship is unacceptable, while the best method during both months uses the square-root relationship with random overlap, temperature-dependent thresholds, and no cloud mask. The fourth-root relationship produces RMS differences that are close to those for the square-root method. Clearly, inclusion of overlap and temperature dependent RHI thresholds produces superior results. The simulations with cloud masks produced similar results and yielded greater RMS differences overall than the simulations that used no cloud mask. Table

Some of the difference is surely attributable to errors in the observed contrail coverage. Although thick clouds are expected to obscure some of the observed coverage, the objective retrieval can also overestimate contrail coverage in cloudy areas because it identifies cloud streets and cirrus streamers as contrails (e.g., MINNIS et al. 2004). A manual analysis of randomly selected results from 2 months of the CONUS satellite analyses (PALIKONDA et al. 2004) indicated that the objective contrail detection algorithm missed an additional 5 and 10 % of contrails. However, nearly 50 - 60% of all pixels identified as contrails were judged to be other cloud features such as cumulus cloud streets and cirrus streamers for those two months (April and July 2001). The greatest overestimates occurred over Canada and outlying ocean areas

suggesting that the errors were smaller over the CONUS. Better regional and overall quantification of the errors are needed to fully assess how much of the RMS difference in Table 1 is due to the observations.

More satellite data must also be analyzed and additional model simulations are needed to help understand interannual and diurnal variability in both PCF and contrail coverage. The results from PALIKONDA et al. (2004) were taken during 2001 when the upper troposphere over the CONUS was unusually dry. Additionally, the initial comparisons of the *NOAA-15* and *NOAA-16* contrail coverage estimates from 2001 (Palikonda et al. 2004) suggest that the relationship between detectable contrails and air traffic might vary with time of day because of saturation effects. That is, more contrails form in the morning when the upper troposphere is cleaner and has been crossed by relatively few airplanes during the previous 6 hours. During the afternoon, the air that was susceptible to contrail formation early in the morning has either been saturated with contrails and their antecedent cirrus clouds to some extent by the hours of passing air traffic or the excess moisture in the relevant altitudes has been reduced significantly by precipitation of the contrail ice crystals formed earlier in the day. The results from other satellite platforms such as *NOAA-15* and the NASA *Terra*, with crossover times approximately 7 and 4 hours before *NOAA-16*, would help determine whether the relation between contrail coverage and air traffic truly changes throughout the day. That type of variation would need to be included in any simulation. Simulations of other months of data will also help to determine the cause of the regional differences between the observed and simulated coverages during the two months presented above.

To improve the simulated coverages, more comparisons are needed between satellite-based estimates of contrail coverage and the PCFs diagnosed from RUC analyses and other

numerical weather analyses. Numerical weather prediction models are not designed with an emphasis on accurate upper tropospheric humidity. Although an improvement over radiosonde measurements, models such as the RUC40 still have a dry bias in relative humidity in the upper troposphere. The use of a temperature-dependent RHI threshold appeared to improve the comparison between the simulated and observed coverages. Significant changes in the model physics as seen in the RUC20 results (Figure 4) profoundly affect the computation of PCF and must be considered in future studies. Most ice supersaturations have been eliminated from the current RUC20 analyses, and new schemes to relate contrail persistent formation to the meteorological variables must be developed. Comparisons of RUC-based PCF with contrail observations will help in the development of these schemes, and to determine areas where the RUC has difficulties in analyzing relative humidity. Meanwhile, other numerical weather analysis results should be tested in this simulation scheme to determine if they can provide any better accuracy than found with the RUC40 results.

Two factors not addressed here but implied from the results presented above may have important effects on contrail coverage. The differences between the observed and simulated coverages over the Great Plains suggest that the effects of synoptic-scale vertical motions may be important to the development of contrails and must be included in future studies. Contrail advection has also not been considered, and may account for the larger observed coverages off the eastern coast of the CONUS as contrails advect from a large area of high traffic density to the Atlantic.

6. Concluding Remarks

The square-root simulations produce a better match with the observations than the simple linear simulations, and reduce some of the differences between simulated and observed contrail coverages over the CONUS. More work remains to determine how much of the contrail coverage pattern is influenced by the air traffic density versus the upper tropospheric conditions reflected in the PCF. Sensitivity to other factors including aircraft type (engine efficiency) and numerical weather analysis source should also be tested. It is likely that the differences between simulated and observed contrail coverage will be reduced further using the suggested tests and improvements.

The framework developed here for simulating contrails in a realistic fashion will be extremely valuable not only for diagnosing linear contrail formation but also for examining parameterizations of contrail spreading and contrail optical properties, parameters necessary for determining and predicting contrail climate effects. By comparisons with the observed contrails, the simulations should be useful for providing data need to correct biases in upper tropospheric humidity, a variable that could ultimately improve weather forecasts. Because the methodology described in this study is based on hourly numerical weather analyses, it is possible to apply it in near-real time or in a forecast mode using predictions instead of analyses. If operated in a predictive fashion, it would be possible to confidently prognosticate those altitudes and areas where contrail outbreaks are likely. With such information, it should be possible for air traffic controllers to reroute some of the upcoming flights to avoid the areas of potential contrail coverage and mitigate some of the potential climate impacts of air travel while conserving fuel in areas when contrail formation potential is low. Much additional research is required, however, to reach the level of confidence needed for implementation of contrail prediction scheme, an act

that would certainly disrupt many aspects of the present air traffic system. Nevertheless, the prototype contrail diagnosis model presented in this study represents an important step in developing accurate contrail forecasts and the effects of contrails on climate.

Acknowledgements. This research was supported by grants NASA NAG-1-2135 and NAG-1-02044, the NASA Pathfinder Program and the NASA Radiation Sciences Program. The authors wish to thank Yan Chen for providing the ice cloud coverage figures.

References

- ALDUCHOV, O. A., R. E. ESKRIDGE, 1996: Improved Magnus form approximation of saturation vapor pressure. — *J. Appl. Meteorol.*, **35**, 601-609.
- APPLEMAN, H., 1953: The formation of exhaust condensation trails by jet aircraft. — *Bull. Amer. Meteorol. Soc.*, **34**, 14-20.
- BAKAN, S., M. BETANCOR, V. GAYLER, H. GRABL, 1994: Contrail frequency over Europe from NOAA-satellite images. — *Ann. Geophys.*, **12**, 962-968.
- BARNES, W. L., T. S. PAGANO, and V. V. SALOMONSON, 1998: Prelaunch characteristics of the Moderate Resolution Imaging Spectroradiometer (MODIS) on EOS-AM1. *IEEE Trans. Geosci. Remote Sens.*, **36**, 1088-1100
- BENJAMIN, S. G., J. M. BROWN, K. J. BRUNDAGE, D. DÉVÉNYI, G. A. GRELL, D. KIM, B. E. SCHWARTZ, T. G. SMIRNOVA, T. L. SMITH, S. S. WEYGANDT, and G. S. MANIKIN, 2004: An hourly assimilation/forecast cycle: The RUC. — *Mon. Wea. Rev.*, **131**, in press.
- BJORNSON, B. M., 1992: SAC contrail formation study. — USAFETAC/PR--92/003, USAF Environmental Technical Applications Center, Scott Air Force Base, Illinois 62225-5438.
- BUSEN, R., U. SCHUMANN, 1995: Visible contrail formation from fuels with different sulfur contents. — *Geophys. Res. Lett.*, **22**, 1357-1360.
- DUDA, D. P., P. MINNIS, L. NGUYEN, R. PALIKONDA, 2004: A case study of the development of contrail clusters over the Great Lakes. — *J. Atmos. Sci.*, in press.
- GARBER, D. P., P. MINNIS, K. P. COSTULIS, 2004: A USA commercial flight track database for upper tropospheric aircraft emission studies. — *Meteorol. Z.*, submitted.
- MANNSTEIN, H., R. MEYER, P. WENDLING, 1999: Operational detection of contrails from NOAA-AVHRR data. — *Int. J. Remote Sensing*, **20**, 1641-1660.

- MEYER, R., H. MANNSTEIN, R. MEERKÖTTER, U. SCHUMANN, P. WENDLING, 2002: Regional radiative forcing by line-shaped contrails derived from satellite data. — *J. Geophys. Res.*, **107**, 10.1029/2001JD000426.
- MILOSHEVICH, L. M., H. VÖMEL, A. PAUKKUNEN, A. J. HEYMSFIELD, and S. J. OLTMANS, 2001: Characterization and correction of relative humidity measurements from Vaisala RS80-A radiosondes at cold temperatures. — *J. Atmos. Oceanic Technol.*, **18**, 135-156.
- MINNIS, P., R. PALIKONDA, B. J. WALTER, J. K. AYERS, and H. MANNSTEIN, 2004: Contrail coverage over the North Pacific from AVHRR data. — *Meteorol. Z.*, submitted.
- MINNIS, P., U. SCHUMANN, D. R. DOELLING, K. M. GIERENS, D. W. FAHEY, 1999: Global distribution of contrail radiative forcing. — *Geophys. Res. Lett.*, **26**, 1853-1856.
- MINNIS, P., D. F. YOUNG, B. A. WIELICKI, D. P. KRATZ, P. W. HECK, S. SUN-MACK, Q. Z. TREPTE, Y. CHEN, S. L. GIBSON, R. R. BROWN, 2002: Seasonal and diurnal variations of cloud properties derived for CERES from VIRS and MODIS data. — *Proc. 11th Conf. Atmospheric Radiation*, Ogden, Utah, Amer. Meteorol. Soc., Boston, 20-23.
- PALIKONDA, R., P. MINNIS, D. R. DOELLING, P. W. HECK, D. P. DUDA, H. MANNSTEIN U. SCHUMANN, 1999: Potential radiative impact of contrail coverage over continental USA estimated from AVHRR data. — *Proc. 10th Conf. Atmospheric Radiation*, Madison, Wisconsin, Amer. Meteorol. Soc., Boston, 181-184.
- PALIKONDA, R., P. MINNIS, D. P. DUDA, B. J. WALTER, and H. MANNSTEIN, 2004: Contrail coverage over the United States of America during 2001 derived from AVHRR data. — *Meteorol. Z.*, submitted.

PONATER, M., S. MARQUART, R. SAUSEN, 2002: Contrails in a comprehensive global climate model: Parameterization and radiative forcing results. — *J. Geophys. Res.*, **107**, 10.1029/2001JD000429.

SAUSEN, R., K. GIERENS, M. PONATER, U. SCHUMANN, 1998: A diagnostic study of the global distribution of contrails. Part I: Present day climate. — *Theor. Appl. Climatol.*, **61**, 127-141.

SCHRADER, M. L., 1997: Calculations of aircraft contrail formation critical temperatures. — *J. Appl. Meteor.*, **36**, 1725-1729.

Table Captions

Table 1. Root-mean-square (RMS) differences between the observed CONUS contrail coverage and several simulated contrail coverages. Simulations are specified by contrail coverage/air traffic relationship (linear/sqroot/4throot), RHI threshold (temperature dependent/100/85), vertical resolution (no overlap (1 layer) /overlap (4 layers)), and cloud mask (all cloud/thick cloud/high cloud/no cloud). All RMS differences are in percent.

Table 1

September 2001

Simulation				RMS difference (%)
sqrt	temp	overlap	no cloud (Figure 5c):	0.274
sqrt	temp	no overlap	no cloud:	0.287
4 th root	temp	overlap	all cloud:	0.295
sqrt	temp	overlap	all cloud:	0.313
sqrt	100	no overlap	no cloud:	0.289
sqrt	100	overlap	no cloud:	0.315
sqrt	100	overlap	thick cloud:	0.351
sqrt	100	overlap	high cloud:	0.363
sqrt	100	overlap	all cloud:	0.399
sqrt	85	overlap	all cloud:	0.317
sqrt	100	no overlap	all cloud:	0.360
linear	100	no overlap	all cloud (Figure 5a):	0.403

November 2001

Simulation				RMS difference (%)
sqrt	temp	overlap	no cloud (Figure 6c):	0.603
sqrt	temp	no overlap	no cloud:	0.597
4 th root	temp	overlap	all cloud:	0.630
sqrt	temp	overlap	all cloud:	0.697
sqrt	100	no overlap	no cloud:	0.633
sqrt	100	overlap	no cloud:	0.664
sqrt	100	overlap	thick cloud:	0.750
sqrt	100	overlap	high cloud:	0.753
sqrt	100	overlap	all cloud:	0.792
sqrt	85	overlap	all cloud:	0.703
sqrt	100	no overlap	all cloud:	0.775
linear	100	no overlap	all cloud (Figure 6a):	0.933

Figure Captions

Figure 1. (a) Ice-cloud amount computed from *Terra* MODIS daytime observations during September 2001. (b) Same as (a), but for November 2001.

Figure 2. (a) Potential persistent contrail frequency computed from RUC analyses for September 2001. (b) Same as (a), but for November 2001.

Figure 3. (a) Potential persistent contrail frequency computed from RUC analyses during available *NOAA-I6* afternoon overpass times for September 2001. (b) Same as (a), but for November 2001.

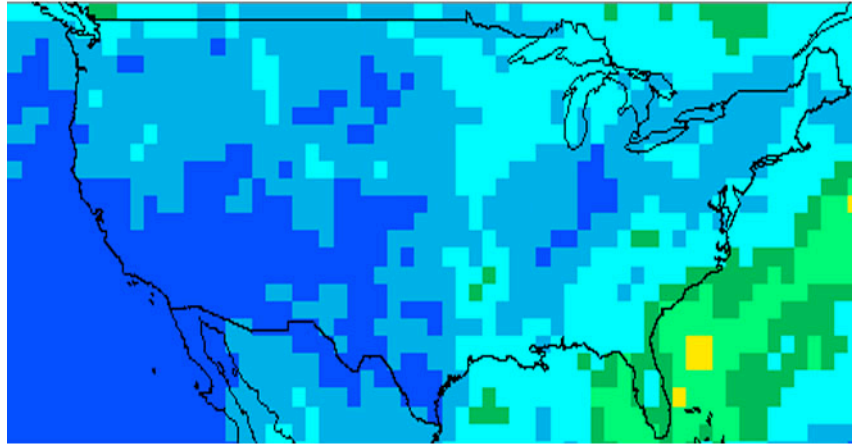
Figure 4. Time series of potential contrail frequency computed from RUC analyses between December 2000 and April 2003. The solid line is the frequency computed for all RUC grid points, while the dashed line only includes grid points over the CONUS. The dotted line indicates the *GOES-8* observation index.

Figure 5. (a) Persistent contrail coverage computed for September 2001 assuming linear relationship between contrail coverage and air traffic density, constant RHI threshold (100%), and high cloud mask. (b) Contrail coverage computed from *NOAA-I6* afternoon overpasses for September 2001 using an objective analysis. (c) Persistent contrail coverage computed for September 2001 assuming a square root relationship between contrail coverage and air traffic density, temperature-dependent RHI threshold, and no cloud mask. Contrail coverage is calculated within four equally spaced layers between 7 and 15 km with random overlap between layers.

Figure 6. Same as Fig. 5, but for November 2001.

Figure 7. (a) Observed minus square-root simulated contrail coverage over the continental US for September 2001. (b) Same as (a), but for November 2001.

a) September 2001



b) November 2001

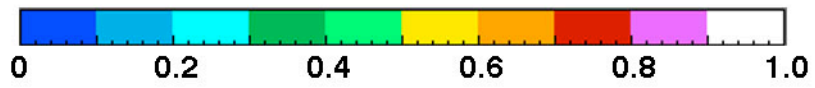
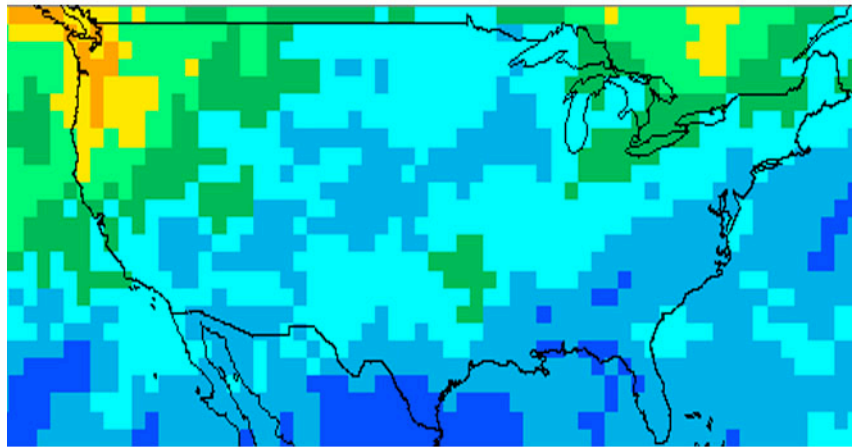
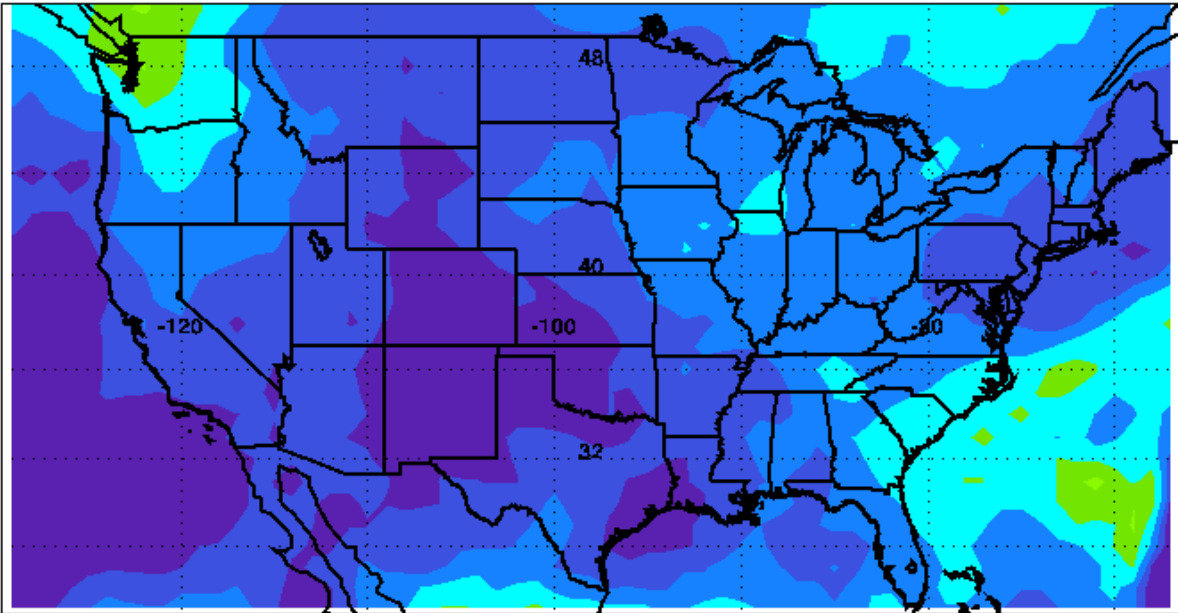


Figure 1

a) September 2001 PCF



b) November 2001 PCF

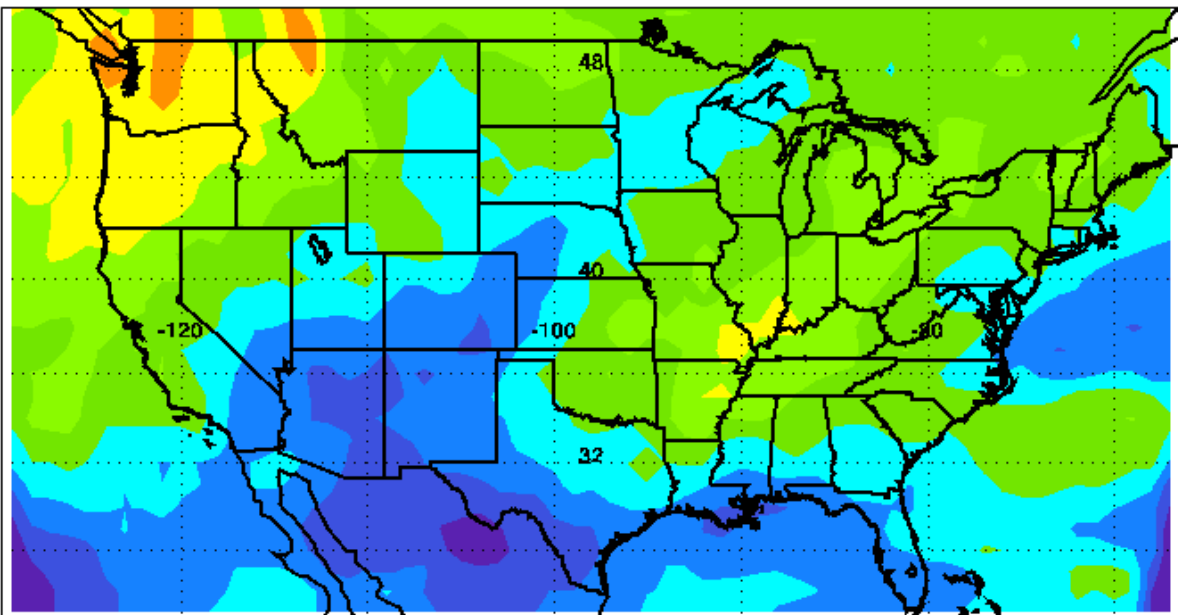
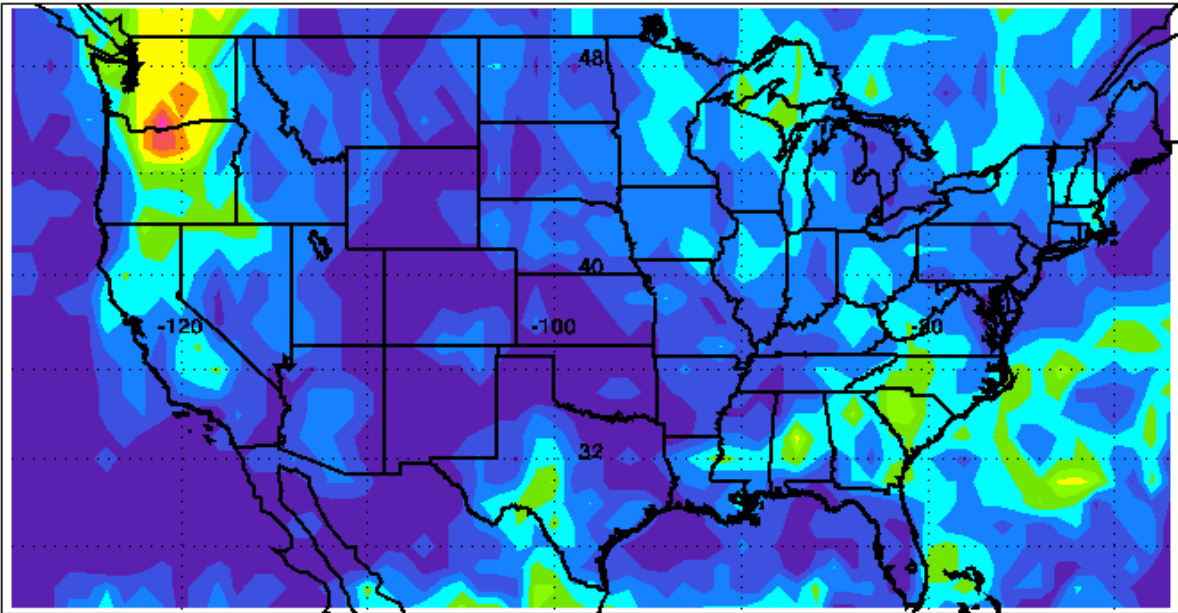


Figure 2

a) PCF in N-16 overpass areas - September 2001



b) PCF in N-16 overpass areas - November 2001

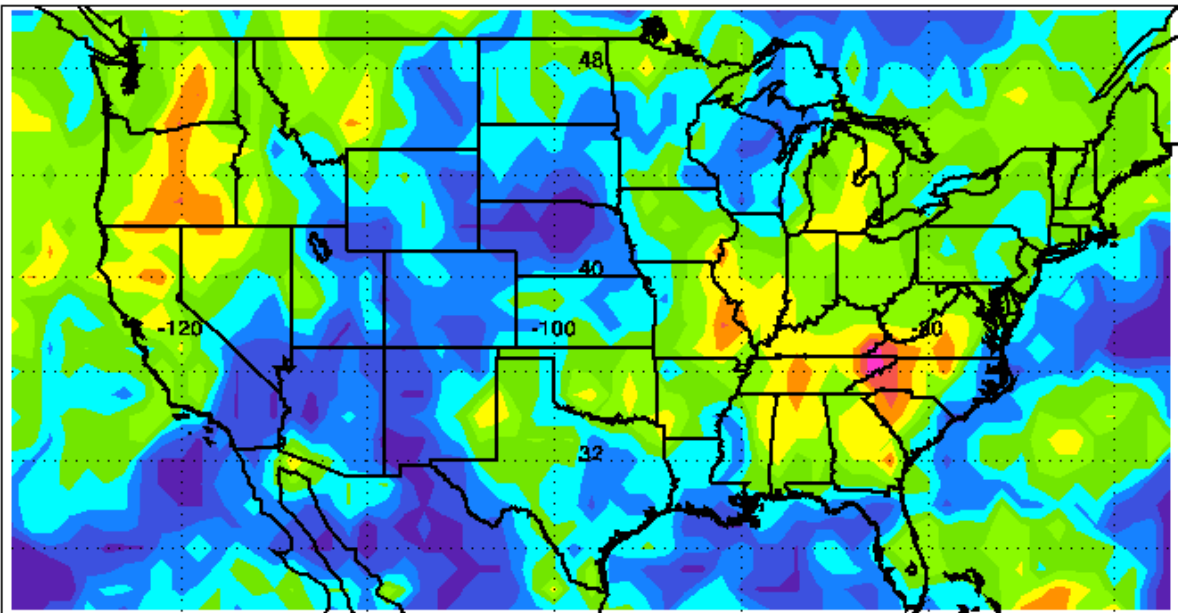


Figure 3

RUC-based Potential CT Frequency

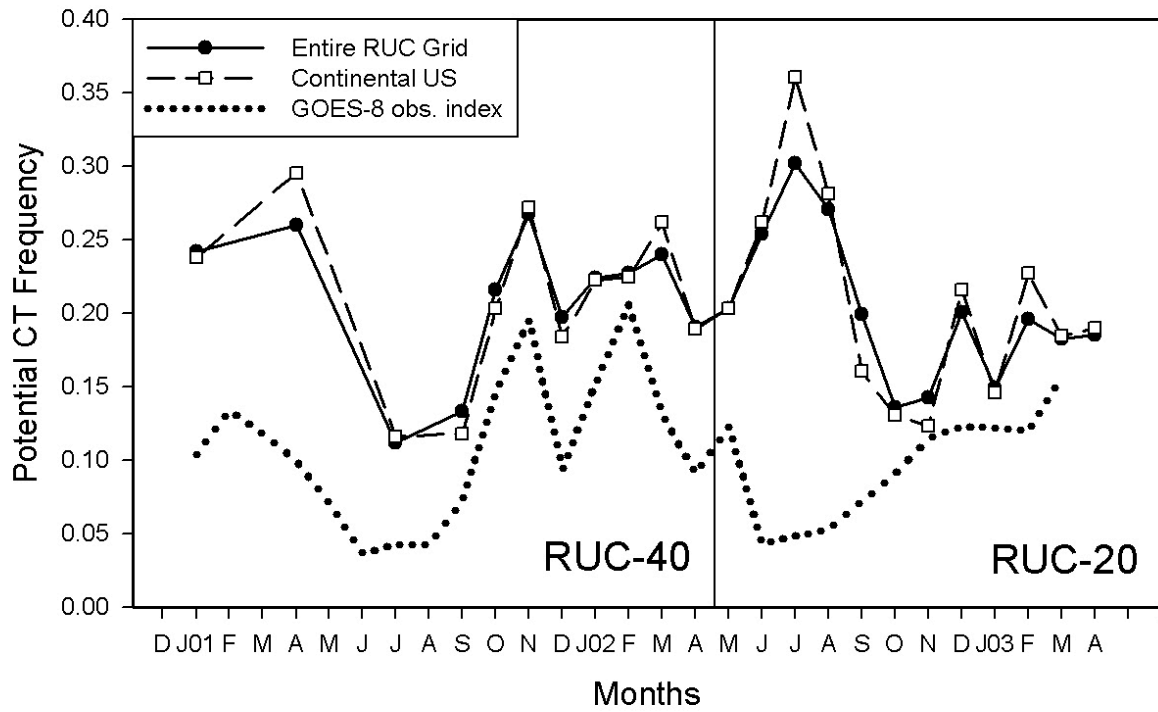
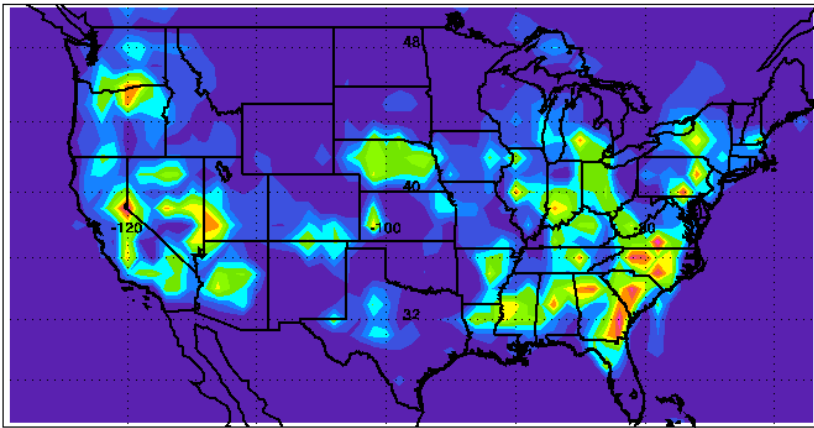
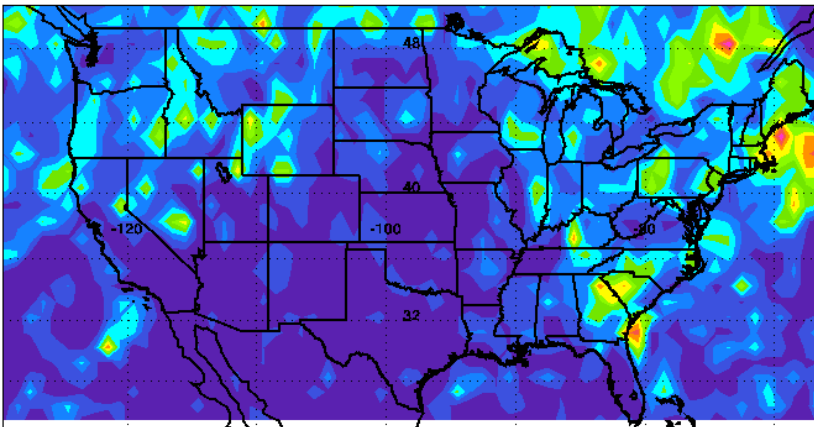


Figure 4

a) linear simulated



b) NOAA-16 observed



c) square-root simulated

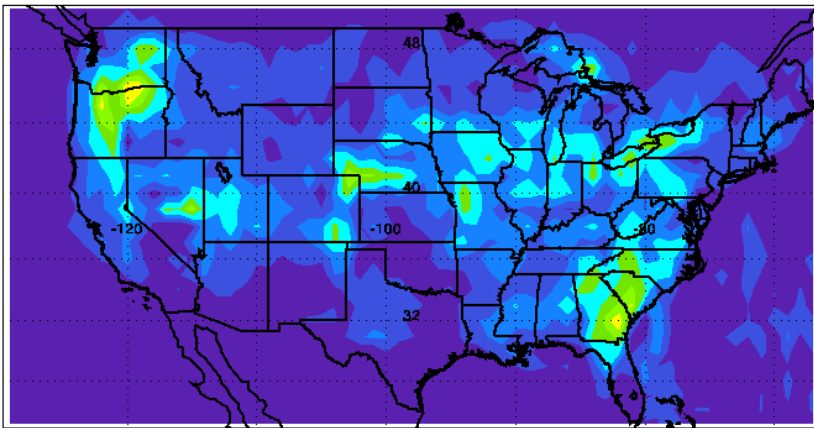
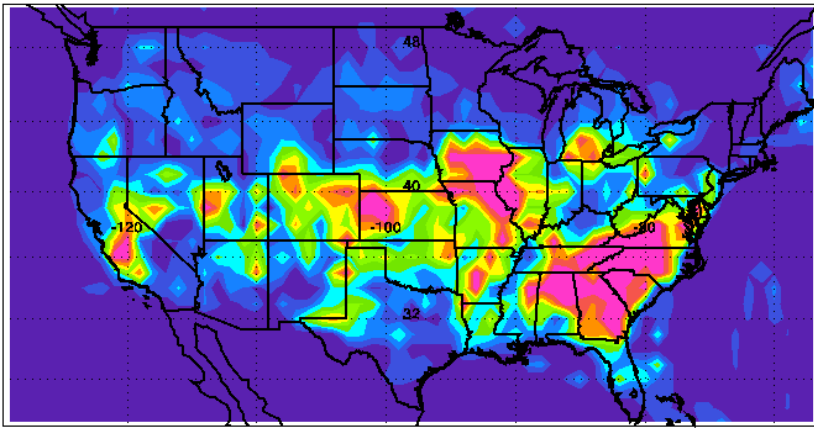
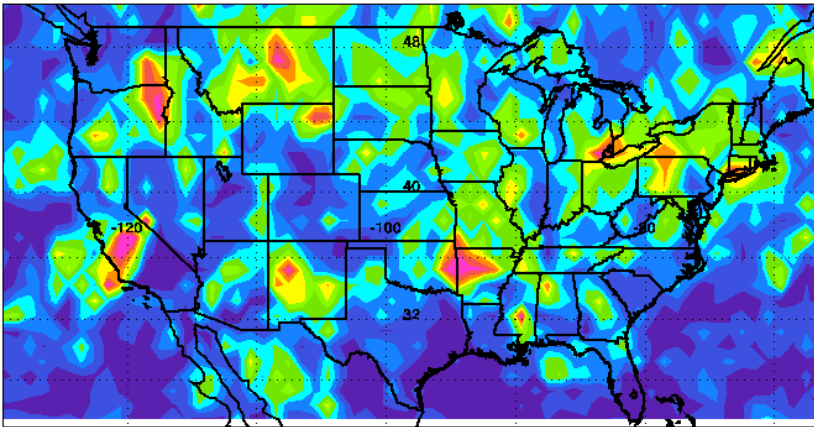


Figure 5

a) linear simulated



b) NOAA-16 observed



c) square-root simulated

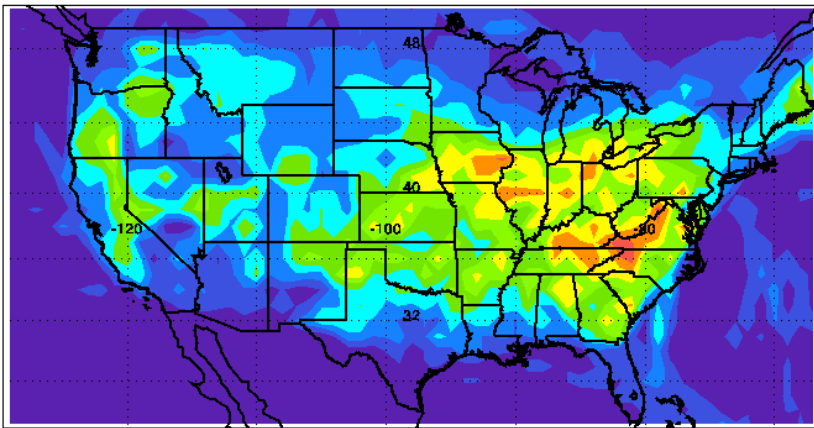
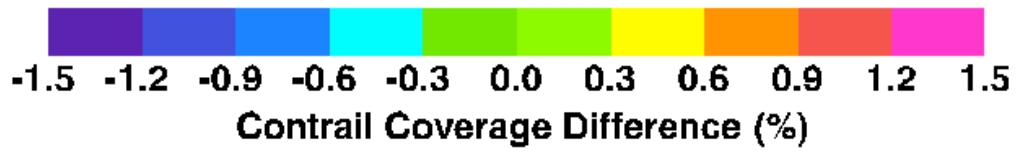
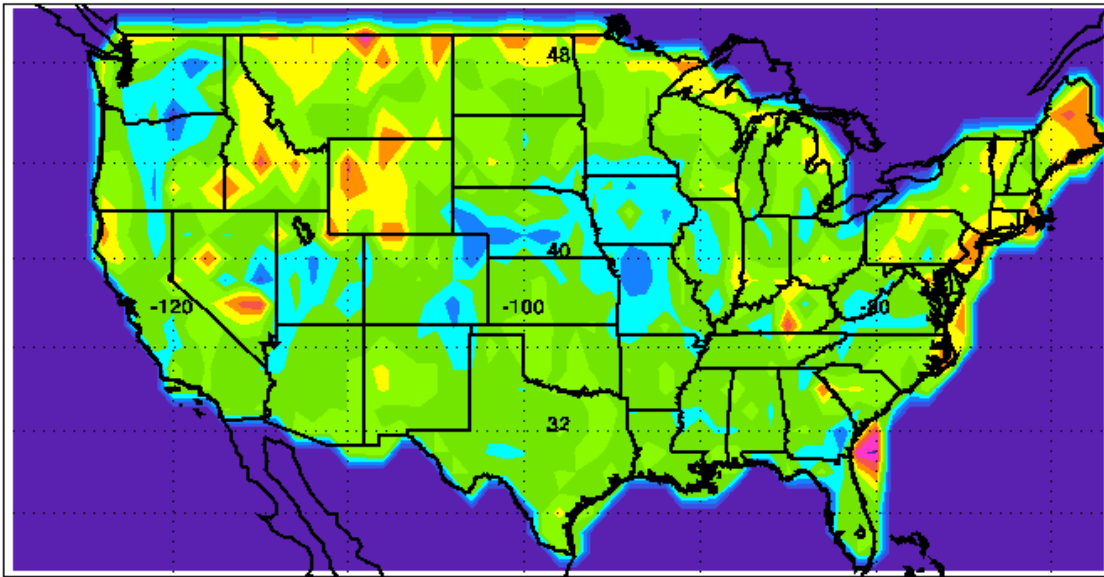


Figure 6

a) satellite minus simulated - September 2001



b) satellite minus simulated - November 2001

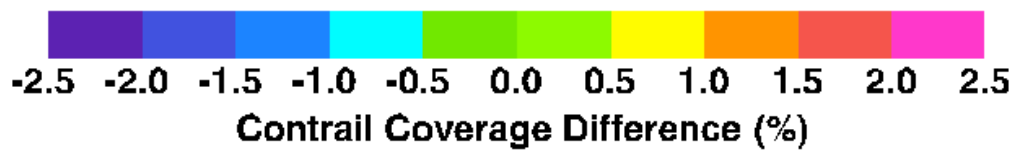
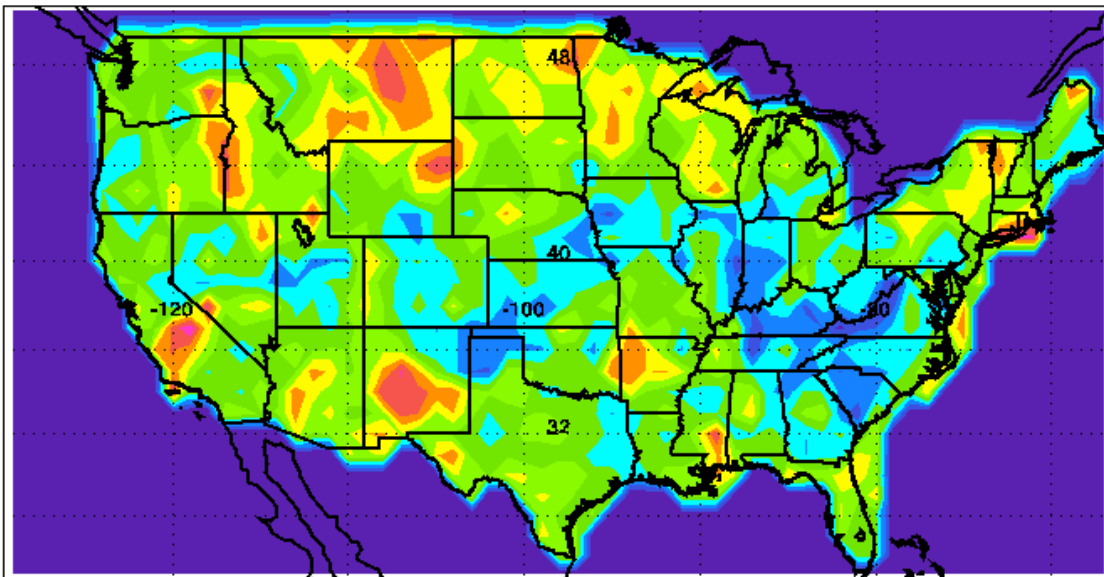


Figure 7